Quantitative relationships between river and channel-belt planform patterns

Tian Y. Dong[1] and Timothy A. Goudge[1,2]

[1] *Jackson School of Geosciences, University of Texas at Austin, Austin, Texas 78712, USA*

[2] *CIFAR Azrieli Global Scholars Program, CIFAR, Toronto, Ontario, Canada*

ABSTRACT

Channel planform patterns arise from internal dynamics of sediment transport and fluid flow in rivers and are affected by external controls, like valley confinement. Understanding whether these channel patterns are preserved in the rock record has critical implications for our ability to constrain past environmental conditions. Rivers are preserved as channel-belts, which are one of the most ubiquitous and accessible parts of the sedimentary record, yet the relationship(s) between river and channel-belt planform patterns remain unquantified. Here, we analyzed planform patterns of rivers and channel-belts from 30 systems globally. Channel patterns were classified using a graph-theory-based metric, the Entropic Braided Index (eBI), which quantifies the number of river channels by considering partitioning of water and sediment discharge. We find that, after normalizing by river size, channel-belt width and wavelength, amplitude, and curvature of the belt edges, decrease with increasing river channel number (eBI). Active flow in single-channel rivers occupies as little as 1% of the channel-belt, while in multichannel rivers it can occupy >50% of the channel-belt. Moreover, we find that channel patterns lie along a continuum of river channel number. Our findings have implications for studies on river and floodplain interaction, storage timescales of floodplain sediment, and paleoenvironmental reconstruction.

INTRODUCTION

Rivers display a diverse set of planform channel patterns on planetary surfaces, typified by meandering and braided morphologies (Leopold and Wolman, 1960). These patterns emerge from internal dynamics of sediment transport and fluid flow, and external controls like vegetation cover and confinement (Parker, 1976; Limaye and Lamb, 2013; Naito and Parker, 2020). Thus, channel patterns – if preserved in, and accurately interpreted from, the rock record – have the possibility of recording crucial paleoenvironmental information through a planet's history, helping to constrain the past climate, carbon cycling, and habitability (e.g., Ganti et al., 2019).

Through channel migration and avulsion, rivers move laterally away from their present course. Over time, this movement forms channel-belts as the amalgamation of many river courses, recording environmental signals in the stratigraphy (Hajek and Straub, 2017). In planform view, channel-belt deposits, a widely accessible sedimentary record across planets, are observed via a range of imaging techniques, such as seismic, hyperspectral, and LiDAR (e.g., Cardenas et al., 2018; Durkin et al., 2018; Hayden et al., 2019; Zaki et al., 2020). Channel-belt geometries may thus provide readily accessible constraints for paleoenvironmental reconstructions. Previous work has established an empirical relationship between channel-belt width and thickness of channel deposits (Gibling, 2006). Results of numerical and physical experiments also suggest that channel-belt width grows logarithmically, while the growth rate and stable width are sensitive to internal and external controls, such as water discharge and regional slope (Howard, 1996; Jobe et al., 2016; Limaye, 2020).

However, empirical relationships between river and channel-belt planform patterns remain elusive. Previous work on channel-belts has often studied single-channel and multichannel rivers separately (Limaye, 2020; Yan et al., 2021), while in nature, planform channel patterns are unlikely to conform to this binary classification (Galeazzi et. al 2021). Furthermore, while morphodynamic models have the capacity to allow rivers to self-form channel patterns, computation costs prevent these models from simulating deposits over geologic timescales (Nicholas, 2013). Herein we explore the connections between river and channel-belt planform patterns across a range of natural systems. We hypothesize that for multichannel rivers the ratio of channel-belt to channel width will approach unity, while for single-channel rivers this ratio will greatly exceed unity (Figure 1A). To test our hypothesis, we conducted remote sensing analysis on 30 river reaches globally (Figure S1). Results of this study inform future work on the interactions between rivers and their deposits, storage timescales of floodplain material, and paleoenvironmental reconstruction.

METHODS

Measuring channel-belt planform patterns

To study channel-belt planform patterns, we mapped 30 river reaches globally, spanning a range of scale and hydrology (see supplementary for detail). Main remotely sensed datasets used for mapping include Sentinel-2 hyperspectral images and NASA Shuttle Radar Topography Mission digital elevation model. Using these data, channel-belt edges were mapped manually in ArcGIS based on changes in topography, ground texture, and vegetation (see supplementary for detail). For example, channel-belt edges are delineated using elevation difference between the inferred alluvial channel-belt and terraces (Figure 1B), ground texture differences between regions with and without abundant thermokarst lakes near the channel-belt (Figure 1C), and abrupt changes in vegetation from trees/shrubs to bare earth (Figure 1D).

channel-belts planform metrics were measured mainly using a graph-theory-based mapping package RivGraph (Schwenk and Hariharan, 2021; see supplementary for detail). A channel-belt centerline was generated automatically from the mapped belt edges (Figure 2A). Channel-belt width was measured every ~10 m along the centerline using perpendicular transects. Three planform metrics, including wavelength, amplitude, and curvature, were measured from the channel-belt centerline and edges. These metrics were then normalized by the total active channel width to compare rivers across scales and to test our hypothesis (Figure 1A).

Measuring channel planform patterns

A binary water mask was generated for each river using a mosaic of Sentinel-2 data during the wettest month, and a modified version of the normalized difference water index (Figure 2B; Yan et al., 2020; see supplementary for detail). The channel centerline, width, and planform patterns were extracted automatically using RivGraph from the binary mask. Here we quantified channel planform pattern using the channel number calculated from the Entropic Braided Index (eBI), a method that weights each channel by the amount of water/sediment discharge it conveys (Tejedor et al., 2019; Figure 2B):

$$\text{eBI} = 2^{H}. \quad (1)$$

Here, H is Shannon Entropy and is used to approximate the probability of a tracer particle entering a particular channel at a given cross-section. Ideally, H is calculated using water/sediment discharge data, but such data at multiple cross-sections along a river are scarce and challenging to collect. However, channel width has been shown to effectively predict water and sediment discharge under steady and uniform flow conditions (Dong et al., 2020). Thus, H can be expressed in terms of channel width (b_i; Schwenk and Hariharan, 2021):

$$H = -\sum_{i=1}^{N} \frac{b_i}{B} \log_2 \frac{b_i}{B}. \quad (2)$$

Here, i is the ith channel at a sampling cross-section, N is the total number of active channels and B is the sum of individual channel widths at the cross-section (Figure 2B). As eBI approaches one, most of the water and sediment discharge is conveyed in one flow path, thus, a river is considered a single-channel system. Alternatively, when eBI is much larger than one, a river is considered a multichannel system.

RESULTS

To show the variability in our results, here we report the median and interquartile ranges of the normalized channel-belt metrics and eBI along a single reach (Figure 3A). Quantitative relationships between normalized channel-belt metrics and eBI are evaluated via linear least squares regression in logarithmic space. Note that the resulting empirical functions are used solely as a straightforward way to illustrate correlations. We find a relationship between normalized channel-belt width and eBI (Figure 3A). In general, normalized channel-belt width decreases with increasing eBI, consistent with our hypothesis. Said another way: as eBI increases, the active river occupies a larger fraction of the channel-belt. This relationship is also found after binning the data by quartiles of eBI (Figure 3B). For the endmember cases, single-channel rivers (quartile 1, eBI = $1.0^{+0.3}_{-0.0}$) occupy $4.3\%^{+0.8\%}_{-1.1\%}$ of the channel-belt width, while multichannel rivers (quartile 4, eBI = $4.2^{+2.1}_{-1.3}$) occupy $27.4\%^{+5.5\%}_{-7.4\%}$ of the channel-belt width (Table S1). We also find relationships between normalized channel-belt wavelength, amplitude, and curvature, measured from both the channel-belt edges and centerline, and eBI (Figure 4).

However, metrics measured from the channel-belt centerline are nearly one order of magnitude larger than those measured from the channel-belt edges, with consistently lower R^2 values (Figure 4).

DISCUSSION

Quantitative relationships between river and channel-belt planform patterns

Herein, we find that channel-belt width, wavelength, amplitude, and curvature, normalized by total channel width, decrease with increasing eBI (i.e., channel number). These findings indicate that channel-belts, the amalgamation of individual river courses, retain scaling relationships with their formative channel patterns. Our results are also consistent with recent work showing similar curvature-to-width ratios for channels and channel-belts (Hayden et al., 2021).

We also find that river planform patterns lie along a spectrum of channel number, as quantified by eBI (Figures 3 and 4). We argue this is intuitive, since, in essence, channel patterns are a planform expression of barforms in rivers, such that point bars in meandering rivers, while alternating bars in braided rivers (Ikeda, 1984, Sylvester et al., 2019). Theoretically, barform types are themselves well predicted by continuous hydraulic parameters, such as the Froude Number, and sediment transport metrics, such as the particle Reynolds Number (Ohata et al., 2017). Further, since eBI measures channel number based on water and sediment discharge, this index is expected to describe channel pattern in a continuum (Tejador et al., 2019), as shown for natural systems here (Figures 3 and 4). Compared to previous qualitative classifications, eBI offers a more physics-based description of channel patterns (Galeazzi et al., 2021).

The linkage between barforms and channel patterns can also help explain the differences in the strength of the relationships between wavelength, amplitude, and curvature measured from channel-belt edges and centerline (Figure 4). Channel-belt edges are formed over time by the action of multiple river courses, and thus record the cumulative history of these rivers and their barform dimensions (Gibling, 2006). Planform metrics measured from channel-belt edges are thus expected to contain scaling relationships with channel patterns (Galeazzi et al., 2021). Conversely, the channel-belt centerline can be viewed as a long-wavelength filtered belt edge and so is instead expected to display a muted version of channel pattern information. Thus, the relationships derived from belt centerline are expected to be weaker, as observed (Figure 4).

As eBI approaches one (single-channel rivers), the variability in normalized channel-belt width increases, weakening the overall quantitative relationship (Figure 3A). We hypothesize that this increased variability is due to confinement by bedrock valleys/fluvial terraces. In confined systems, shear stress near the river banks is often not sufficient to overcome the strength of the valley wall material, limiting a river's ability to expand laterally and forcing water and sediment flow into a single pathway, driving incision (Larsen and Lamb, 2016). Thus, normalized channel-belt width would approach unity, even as eBI remains low (Figure 3A). For unconfined systems, rivers can self-organize to form planform patterns based on water and sediment discharge (Parker, 1976).

To test this hypothesis, we parse our data of normalized channel-belt width and eBI based on confinement of the channel-belt, defined as the elevation difference between the channel-belt and its surrounding valley, normalized by the standard deviation of channel-belt elevation (inspired by Limaye and Lamb, 2013; see supplementary for detail). A subset of unconfined channel-belts shows a stronger relationship between channel-belt width and eBI ($R^2 = 0.84$;

Figure S6B), while a subset of confined systems shows no correlation between these two metrics ($R^2 = 0.00$; Figure S6D), confirming our hypothesis.

As an alternative hypothesis, the observed variability in normalized channel-belt width at low eBI could also be due to age differences among the mapped river systems, where older rivers have developed a larger channel-belt. However, the exact ages of mapped channel-belts are unknown, and the timescale for channel-belt width to reach a stable value remains an open question. Further, it is unclear why this age trend would be observed for low eBI (single-channel) rivers, but not high eBI (multichannel) rivers. Despite the causes of variability, like most geomorphic systems, channel-belt width is subject to external impacts of valley confinement, while also retaining signals of internal dynamics of sediment transport and fluid flow (Parker, 1976; Hajek and Straub, 2017).

Implications for river-channel-belt dynamics, stratigraphy, and paleoenvironmental reconstruction

Unconfined, single-channel rivers occupy as little as 1% of the channel-belt width (Figure 3A), implying limited interaction between the active river channel and the channel-belt. While single-channel rivers migrate/avulse laterally, the timescale for a river to visit everywhere in a channel-belt is on the order of centuries to millennia (Jerolmack and Mohrig, 2007), implying that significant portions of the channel-belt have limited fluvial sedimentation, and so can remain as topographic lows. Meanwhile, areas of the channel-belt adjacent to the active river aggrade to become topographic highs, promoting compensational stacking (Hajek and Straub, 2017; Jobe et al., 2020). In contrast, unconfined, multichannel systems can occupy over 50% of the channel-belt width (Figure 3A), implying a greater interaction between river and the channel-belt. Thus, the overall deposits likely contain a greater fraction of channel deposits with smaller topographic variability, consistent with previous findings that braided systems contain more spatially connected channels in the stratigraphy (Bridge and Leeder, 1979).

Interaction between the active river and channel-belt deposits also has important implications for sediment storage timescales, affecting the terrestrial component of the organic carbon cycle. Previous studies have found that sediment storage timescale is well described by heavy-tail distributions in unconfined meandering rivers, indicating preferential erosion of young floodplain material (e.g., Torres el., 2017). This conclusion is consistent with our observations that indicate unconfined single-channel rivers occupy a small fraction of the channel-belt width, thus, decreasing the probability that the active river could interact with older deposits. However, for confined or multichannel rivers, the active river occupies a much larger fraction of the channel-belt, likely reducing the age bias in fluvial erosion. It is thus reasonable to hypothesize that for these types of systems the probability distribution of sediment storage timescale would be light tailed (Wohl 2011; Huffman et al., 2021). Particularly, confined or multichannel rivers might export a greater amount of black carbon to the ocean, affecting residence timescales of organic carbon in the ocean (Masiello, 2004).

Given the prominence of channel-belt deposits in the rock record, the relationships developed herein can be used to inform studies on past environmental changes. For example, our findings could be readily applied to analysis of commonly observed channel-belts deposits from subsurface data (Gibling, 2006), or channel-belt deposits observed across Mars (Cardenas et al., 2020; Dickson et al., 2021), to reconstruct past channel patterns and environments.

ACKNOWLEDGMENTS

This material is based upon work supported by NSF under Award No. 1952814 to T. Dong. We are grateful for insightful reviews by Jason Muhlbauer, Zane Jobe, and an anonymous reviewer. T. Dong thanks C. Qiu and W. Liu for the love and support during writing of this work.

FIGURE CAPTIONS

Figure 1 (A) Cartoon showing two end member cases of river and channel-belt planform patterns: multichannel (left) and single-channel (right) systems. Four planform channel-belt metrics (shown in red) are measured from channel-belt centerline and edges: width, wavelength, amplitude, and curvature. Hypotheses are shown in black boxes. Examples of mapping channel-belt edges using (B) elevation differences at Jurua River, Brazil, (C) ground texture at Kuparuk River, Alaska, and (D) vegetation differences at Niobrara River, Nebraska. White arrows indicate exemplified features for each panel.

Figure 2 (A) A binary water mask generated using a modified normalized difference water index for the Missouri River. (B) The concept of Entropic Braided Index illustrated by three idealized river channel networks (after Tejedor et al., 2019). Red boxes are hypothetical survey locations.

Figure 3 (A) Relationship between median normalized channel-belt width and eBI, shown by the gray circles. Colored squares are median values of data binned by quartiles of eBI. Error bars show interquartile range. Red lines indicate the percentage of channel-belt width occupied by the active river, which is simply the inverse of normalized channel-belt width times 100%. (B) Probability distributions of normalized channel-belt width in each quartile of eBI, corresponding to the colored squares in panel A. Vertical lines are median.

Figure 4 Relationships between median normalized channel-belt (A) wavelength, (B) amplitude, and (C) curvature and eBI. Different symbols represent metrics measured from the channel-belt edges or centerline. Error bars show interquartile range.

REFERENCES CITED

Bridge, J.S. and Leeder, M.R., 1979. A simulation model of alluvial stratigraphy. Sedimentology, v. 26, p. 617-644, https://doi.org/10.1111/j.1365-3091.1979.tb00935.x

Cardenas, B.T., Mohrig, D., Goudge, T.A., Hughes, C.M., Levy, J.S., Swanson, T., Mason, J. and Zhao, F., 2020. The anatomy of exhumed river ‐ channel belts: Bedform to belt ‐ scale river kinematics of the Ruby Ranch Member, Cretaceous Cedar Mountain Formation, Utah, USA. Sedimentology, v. 67, p. 3655-3682, https://doi.org/10.1111/sed.12765

Cardenas, B.T., Mohrig, D. and Goudge, T.A., 2018. Fluvial stratigraphy of valley fills at Aeolis Dorsa, Mars: Evidence for base-level fluctuations controlled by a downstream water body. Bulletin, v. 130, p.484-498, https://doi.org/10.1130/B31567.1

Dickson, J.L., Lamb, M.P., Williams, R.M.E., Hayden, A.T. and Fischer, W.W., 2021. The global distribution of depositional rivers on early Mars. Geology, v. 49, p.504-509, https://doi.org/10.1130/G48457.1

Dong, T.Y., Nittrouer, J.A., McElroy, B., Il'icheva, E., Pavlov, M., Ma, H., Moodie, A.J. and Moreido, V.M., 2020, Predicting water and sediment partitioning in a delta channel network under varying discharge conditions: Water Resources Research, v. 56, p. e2020WR027199, https://doi.org/10.1029/2020WR027199

Durkin, P.R., Hubbard, S.M., Holbrook, J. and Boyd, R., 2018. Evolution of fluvial meander-belt deposits and implications for the completeness of the stratigraphic record. GSA Bulletin, 130(5-6), pp.721-739, https://doi.org/10.1130/B31699.1.

Galeazzi, C.P., Almeida, R.P. and do Prado, A.H., 2021. Linking rivers to the rock record: Channel patterns and paleocurrent circular variance. Geology, v. 49, p.1402-1407, https://doi.org/10.1130/G49121.1

Ganti, V., Whittaker, A.C., Lamb, M.P. and Fischer, W.W., 2019. Low-gradient, single-threaded rivers prior to greening of the continents. Proceedings of the National Academy of Sciences, v. 116, p.11652-11657, https://doi.org/10.1073/pnas.1901642116

Gibling, M.R., 2006. Width and thickness of fluvial channel bodies and valley fills in the geological record: a literature compilation and classification. Journal of sedimentary Research, v. 76, p. 731-770, https://doi.org/10.2110/jsr.2006.060

Hajek, E.A. and Straub, K.M., 2017. Autogenic sedimentation in clastic stratigraphy. Annual Review of Earth and Planetary Sciences, v. 45, p. 681-709, https://doi.org/10.1146/annurev-earth-063016-015935

Hayden, A.T., Lamb, M.P. and Carney, A.J., 2021. Similar curvature-to-width ratios for channels and channel belts: Implications for paleo-hydraulics of fluvial ridges on Mars. Geology, v. 49, p.837–841, https://doi.org/10.1130/G48370.1

Huffman, M.E., Pizzuto, J.E., Trampush, S.M., Moody, J.A., Schook, D.M., Gray, H.J. and Mahan, S.A., Floodplain Sediment Storage Timescales of the Laterally Confined Meandering Powder River, USA. Journal of Geophysical Research: Earth Surface, p.e2021JF006313, https://doi.org/10.1029/2021JF006313.

Howard, A.D., 1996. Modeling channel evolution and floodplain morphology. Floodplain processes, p.15-62.

Ikeda, S., 1984. Prediction of alternate bar wavelength and height. Journal of Hydraulic Engineering, v. 110, p. 371-386, https://doi.org/10.1061/(ASCE)0733-9429(1984)110:4(371)

Jerolmack, D.J. and Mohrig, D., 2007. Conditions for branching in depositional rivers. Geology, v. 35, p.463-466, https://doi.org/10.1130/G23308A.1

Jobe, Z.R., Howes, N.C. and Auchter, N.C., 2016. Comparing submarine and fluvial channel kinematics: Implications for stratigraphic architecture. Geology, 44(11), pp.931-934, https://doi.org/10.1130/G38158.1.

Jobe, Z.R., Howes, N.C., Straub, K.M., Cai, D., Deng, H., Laugier, F.J., Pettinga, L.A. and Shumaker, L.E., 2020. Comparing aggradation, superelevation, and avulsion frequency of submarine and fluvial channels. Frontiers in Earth Science, 8, p.53, https://doi.org/10.3389/feart.2020.00053

Lapôtre, M.G., Ielpi, A., Lamb, M.P., Williams, R.M. and Knoll, A.H., 2019. Model for the formation of single-thread rivers in barren landscapes and implications for pre-Silurian and martian fluvial deposits. Journal of Geophysical Research: Earth Surface, v. 124, p. 2757-2777, https://doi.org/10.1029/2019JF005156

Larsen, I.J. and Lamb, M.P., 2016. Progressive incision of the Channeled Scablands by outburst floods. Nature, v. 538, p. 229-232, https://doi.org/10.1038/nature19817

Leopold, L.B. and Wolman, M.G., 1960. River meanders. Geological Society of America Bulletin, v. 71, p.769-793, https://doi.org/10.1130/0016-7606(1960)71[769:RM]2.0.CO;2

Limaye, A.B., 2020. How do braided rivers grow channel belts?. Journal of Geophysical Research: Earth Surface, v. 125, p. e2020JF005570, https://doi.org/10.1029/2020JF005570

Limaye, A.B. and Lamb, M.P., 2013. A vector-based method for bank-material tracking in coupled models of meandering and landscape evolution. Journal of Geophysical Research: Earth Surface, v. 118, p. 2421-2437, https://doi.org/10.1002/2013JF002854

Masiello, C.A., 2004. New directions in black carbon organic geochemistry. Marine Chemistry, v. 92, p. 201-213, https://doi.org/10.1016/j.marchem.2004.06.043

Naito, K. and Parker, G., 2020. Adjustment of self-formed bankfull channel geometry of meandering rivers: modelling study. Earth Surface Processes and Landforms, v. 45, p. 3313-3322, https://doi.org/10.1002/esp.4966

Nicholas, A.P., 2013. Modelling the continuum of river channel patterns. Earth Surface Processes and Landforms, v. 38, p.1187-1196, https://doi.org/10.1002/esp.3431

Ohata, K., Naruse, H., Yokokawa, M. and Viparelli, E., 2017. New bedform phase diagrams and discriminant functions for formative conditions of bedforms in open-channel flows. Journal of Geophysical Research: Earth Surface, v. 122, p. 2139-2158, https://doi.org/10.1002/2017JF004290

Parker, G., 1976. On the cause and characteristic scales of meandering and braiding in rivers. Journal of fluid mechanics, v. 76, p.457-480, https://doi.org/10.1017/S0022112076000748

Schwenk, J. and Hariharan, J., 2021, RivGraph: Automatic extraction and analysis of river and delta channel network topology: Journal of Open Source Software, v. 6, p. 2952, https://doi.org/10.21105/joss.02952.

Sylvester, Z., Durkin, P., and Covault, J.A., 2019, High curvatures drive river meandering: Geology, v. 47, p. 263–266, https://doi.org/10.1130/G45608.1.

Tejedor, A., Schwenk, J., Kleinhans, M.G., Carling, P.A. and Foufoula-Georgiou, E., 2019, December. The Braiding Index 2.0: eBI: Abstract EP51E-2163 presented at 2019 Fall Meeting, AGU, San Francisco, California, 9–13 December.

Torres, M.A., Limaye, A.B., Ganti, V., Lamb, M.P., West, A.J. and Fischer, W.W., 2017. Model predictions of long-lived storage of organic carbon in river deposits. Earth Surface Dynamics, v. 5, p.711-730, https://doi.org/10.5194/esurf-5-711-2017

Wohl, E., 2011. Threshold-induced complex behavior of wood in mountain streams. Geology, 39(6), pp.587-590, https://doi-org.ezproxy.lib.utexas.edu/10.1130/G32105.1.

Yan, D., Huang, C., Ma, N. and Zhang, Y., 2020, Improved landsat-based water and snow indices for extracting lake and snow cover/glacier in the tibetan plateau: Water, v. 12, p. 1339, https://doi.org/10.3390/w12051339.

Yan, N., Colombera, L. and Mountney, N.P., 2021. Evaluation of Morphodynamic Controls on the Preservation of Fluvial Meander-Belt Deposits. Geophysical Research Letters, v. 48, p. e2021GL094622, https://doi.org/10.1029/2021GL094622

Zaki, A., Pain, C.F., Edgett, K.S. and Castelltort, S., 2020. Global inventories of inverted stream channels on Earth and Mars, https://doi.org/10.31223/osf.io/ej2xk

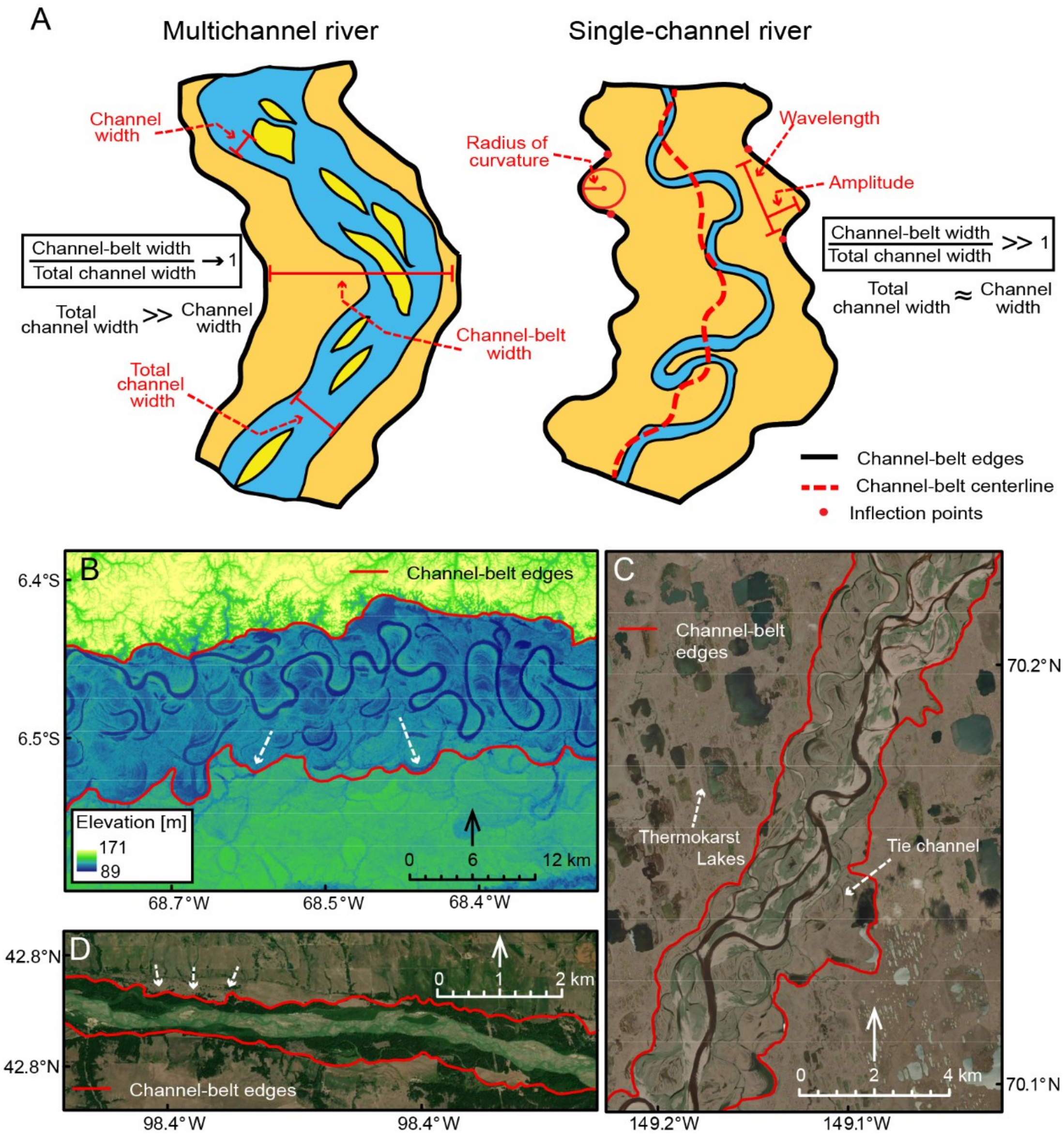

A
Multichannel river
Single-channel river
Channel width
Channel-belt width
Total channel width
→ 1
Total channel width >> Channel width
Channel-belt width
Total channel width
Radius of curvature
Wavelength
Amplitude
Channel-belt width
Total channel width
>> 1
Total channel width ≈ Channel width
Channel-belt edges
Channel-belt centerline
Inflection points
B
Channel-belt edges
6.4°S
6.5°S
Elevation [m]
171
89
0
6
12 km
68.7°W
68.5°W
68.4°W
C
Channel-belt edges
70.2°N
Thermokarst Lakes
Tie channel
0
2
4 km
70.1°N
149.2°W
149.1°W
D
42.8°N
0
1
2 km
42.8°N
Channel-belt edges
98.4°W
98.4°W

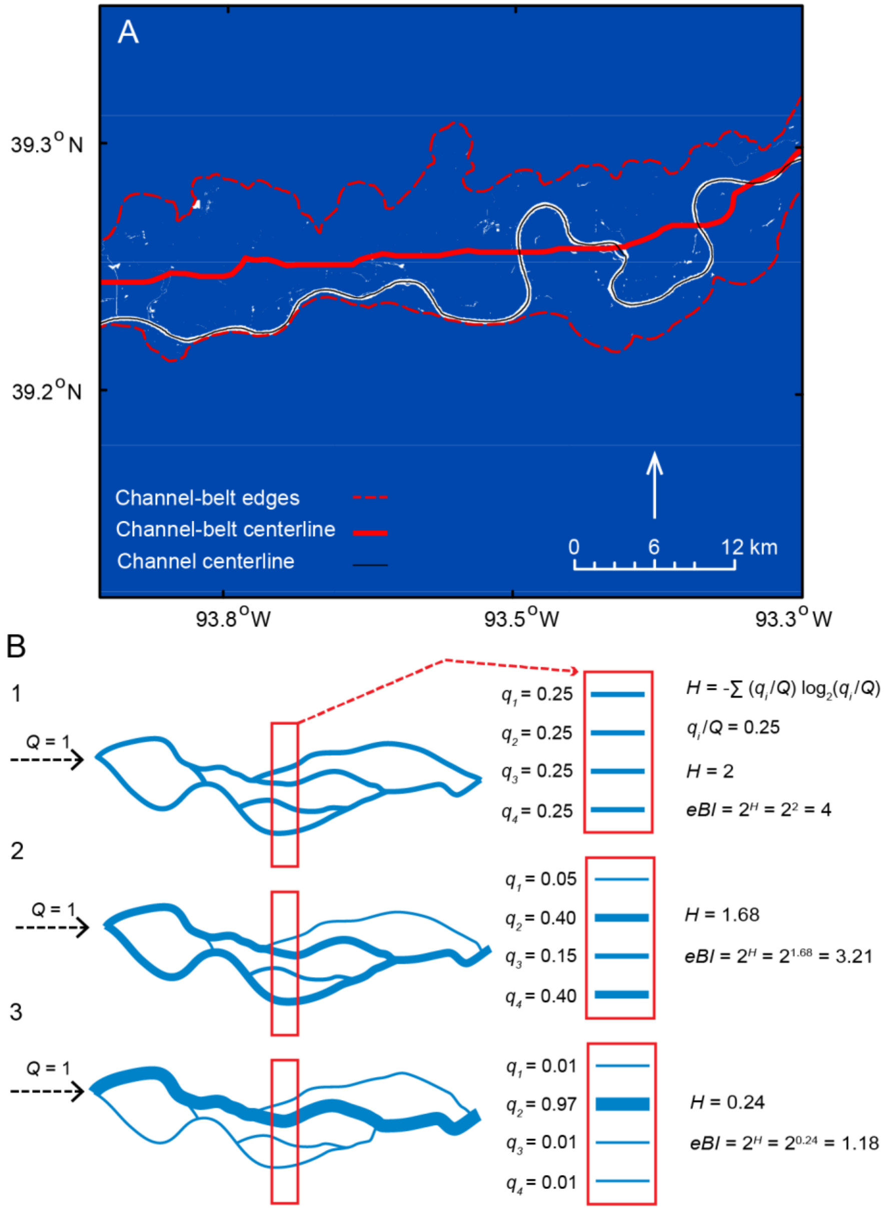
A
39.3° N
39.2° N
93.8° W
93.5° W
93.3° W
Channel-belt edges
Channel-belt centerline
Channel centerline
0
6
12 km
B
1
Q = 1
q_1 = 0.25
q_2 = 0.25
q_3 = 0.25
q_4 = 0.25
$H = -\sum (q_i/Q)\log_2(q_i/Q)$
q_i/Q = 0.25
H = 2
$eBI = 2^H = 2^2 = 4$
2
Q = 1
q_1 = 0.05
q_2 = 0.40
q_3 = 0.15
q_4 = 0.40
H = 1.68
$eBI = 2^H = 2^{1.68} = 3.21$
3
Q = 1
q_1 = 0.01
q_2 = 0.97
q_3 = 0.01
q_4 = 0.01
H = 0.24
$eBI = 2^H = 2^{0.24} = 1.18$

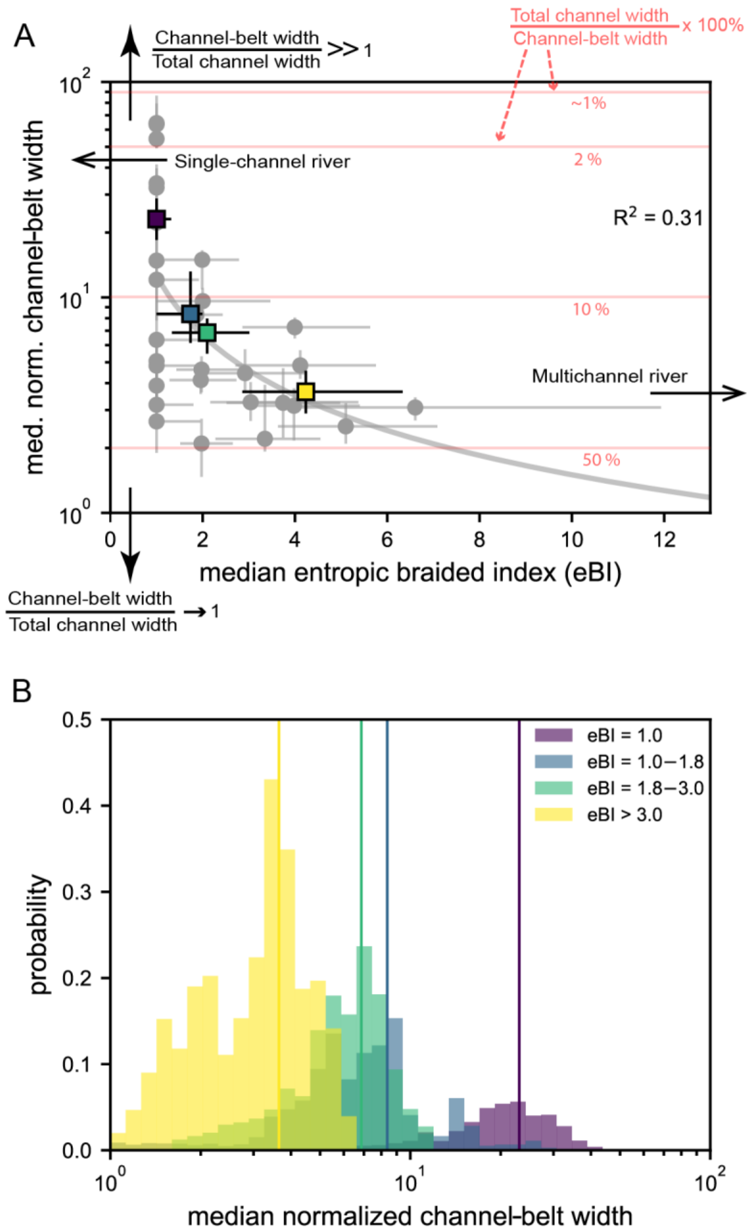

A
Channel-belt width / Total channel width >> 1
Total channel width / Channel-belt width x 100%
~1%
2 %
Single-channel river
R^2 = 0.31
10 %
Multichannel river
50 %
med. norm. channel-belt width
median entropic braided index (eBI)
Channel-belt width / Total channel width → 1
B
eBI = 1.0
eBI = 1.0−1.8
eBI = 1.8−3.0
eBI > 3.0
probability
median normalized channel-belt width

367

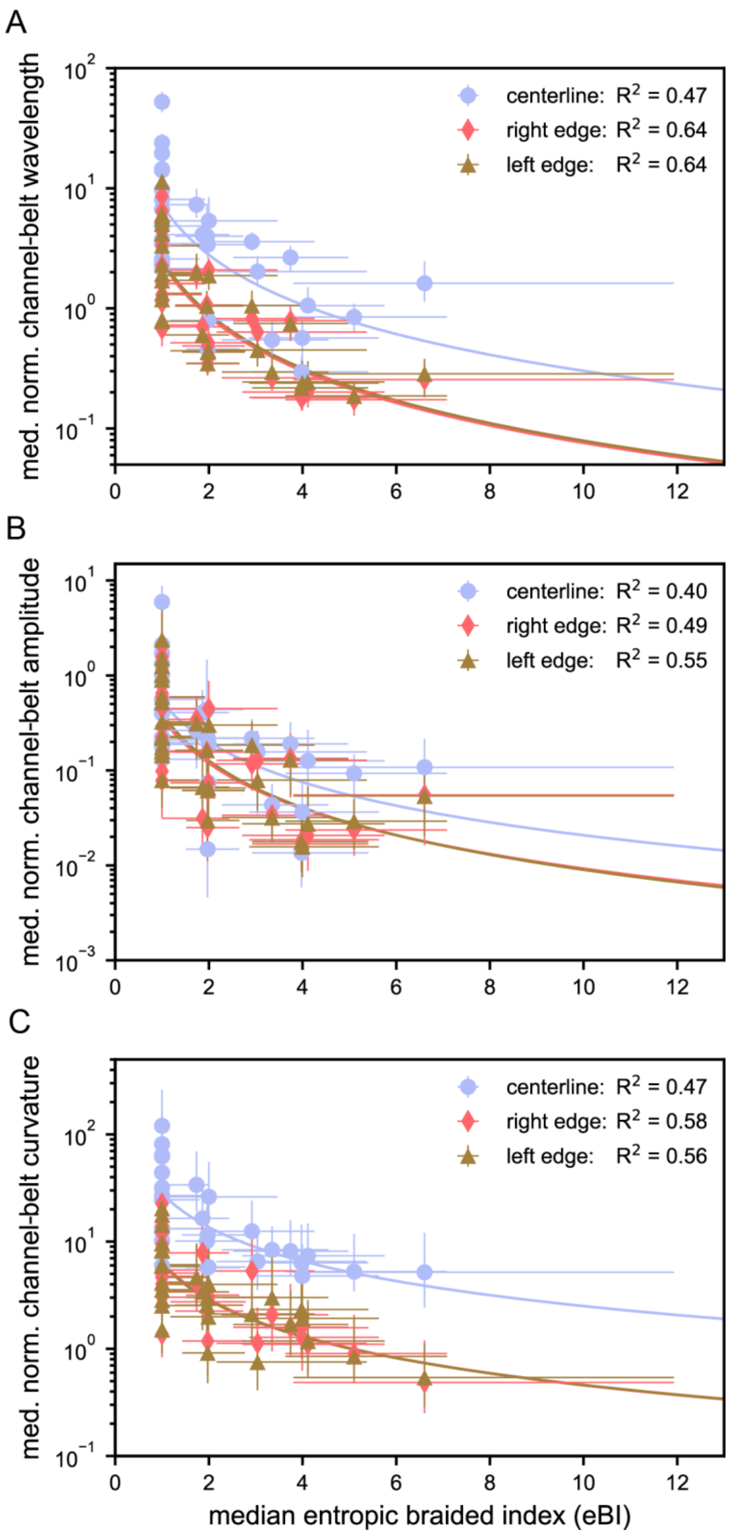
A
med. norm. channel-belt wavelength
centerline: R^2 = 0.47
right edge: R^2 = 0.64
left edge: R^2 = 0.64
B
med. norm. channel-belt amplitude
centerline: R^2 = 0.40
right edge: R^2 = 0.49
left edge: R^2 = 0.55
C
med. norm. channel-belt curvature
centerline: R^2 = 0.47
right edge: R^2 = 0.58
left edge: R^2 = 0.56
median entropic braided index (eBI)